Sixth International Symposium on Turbulence and Shear Flow Phenomena
Seoul, Korea, 22-24 June 2009

HEAT AND MASS TRANSFER ACROSS THE WAVY SHEARED INTERFACE IN WIND-DRIVEN TURBULENCE

Satoru Komori, Ryoichi Kurose and Shuhei Ohstubo
Department of Mechanical Engineering and Science,
Advanced Research Institute of Fluid Science and Engineering,
Kyoto University
Yoshida-Honmachi, Sakyo-ku, Kyoto 606-8501, Japan
komori@mech.kyoto-u.ac.jp, kurose@mech.kyoto-u.ac.jp,
tsuboshu@t01.mbox.media.kyoto-u.ac.jp

Kenji Tanno
Energy Engineering Research Laboratory,
Central Research Institute of Electric Power Industry (CRIEPI)
2-6-1 Nagasaka, Yokosuka, Kanagawa 240-0196, Japan
k-tanno@criepi.denken.or.jp

Naoya Suzuki
Department of Mechanical Engineering,
Kinki University
3-4-1 Kowakae, Higashi-Osaka, Osaka 557-8502, Japan
nsuzuki@mech.kindai.ac.jp

ABSTRACT

Heat and mass transfer mechanism across the sheared air-water interface was both experimentally and numerically investigated. Turbulence structure near the interface was clarified by instantaneous velocity and temperature measurements together with direct numerical simulation of wind-driven turbulence. Heat and mass transfer coefficients on the water side were measured through evaporation and CO_2-desorption experiments in small and large wind-wave tanks and their behaviours against wind speed were discussed with turbulence structure near the interface. The results show that both heat and mass transfer coefficients on the water side increase with the free-stream wind speed and they have a small plateau in the middle wind speed region where the streaky flow structure changes to patchy one. The distributions of the mass transfer coefficient against the free-stream wind speed also show no dependency of fetch and they agree with the field measurements plotted against the free-stream wind speed in the atmospheric surface layer. By using the empirical correlations between the transfer coefficients and the free-stream wind speed the global heat and mass transfer exchange rates across the air-sea interface were estimated. The estimation suggests that the global air-sea heat and mass exchange rates are larger than those predicted by conventional models.

INTRODUCTION

The climate change owing to increasing release of carbon dioxide has been warningly predicted through numerical simulations based on the atmosphere-ocean general circulation model (AOGCM). In order to precisely predict such climate change and abnormal weather, it is of importance to examine some submodels used in the AOGCM without theoretical and experimental verifications.

One of the uncertain submodels is the bulk method for estimating heat and mass transfer across the air-sea interface. The bulk model for estimating CO_2 transfer across the air-sea interface is given by the mass flux per unit area:

$$F = k_L S \Delta pCO_2 , \tag{1}$$

where k_L is the mass transfer coefficient on the water side and S is the solubility of CO_2 in sea water and ΔpCO_2 is the partial pressure difference of CO_2 between atmosphere and ocean. Similarly the total heat flux per unit area Q_T can be estimated on the water side by

$$Q_T = \rho_W C_{p,w} h_L \Delta T , \tag{2}$$

where ρ_W is the water density, $C_{p,w}$ the specific heat of water, h_L the heat transfer coefficient on the water side and ΔT the temperature difference between the interface and bulk water. However, ΔT is so small in oceans that precise data of ΔT cannot be available. Therefore, Q_T for the air-sea interface is estimated on the air side by

$$Q_T = Q_H + Q_E + Q_R , \tag{3}$$

where Q_H is the sensible heat flux, Q_E the latent heat flux and Q_R the radiative heat flux. By using temperatue and specific humidity differences between atmosphere and sea surface, ΔT and Δq, together with sensible and latent heat flux transfer coefficients, C_H and C_E, the sensible and latent heat fluxes, Q_H and Q_E, are given by

$$Q_H = \rho_a C_{p,a} C_H U \Delta T , \tag{4}$$

$$Q_E = \rho_a L_V C_E U \Delta q , \tag{5}$$

where U is the wind speed above the air-sea interface, ρ_G the air density, $C_{p,a}$ the constant pressure specific heat of air and L_V the evaporative latent heat.

The conventional bulk models are based on the assumption that C_H and C_E in Eqs.(4) and (5) are constant irrespective of velocity and temperature fields (DeCosmo et al., 1996) and k_L in Eq.(1) is simply propotional to the mean wind speed at the elevation of 10m from the air-sea interface, U_{10} (Wanninkhof, 1992; McGillis, 2001). However, the values of k_L, C_H and C_E measured in oceans are so scattered among previous studies that it is difficult to verify the assumption in the conventional bulk models.

In order to confirm whether the conventional bulk models are applicable to the estimation of heat and mass flux across the air-sea interface or not, we first have to precisely measure heat and mass fluxes across the sheared wavy air-water interface and to clarify heat and mass transfer mechanism together with turbulence structure near the interface. One of the best ways for getting reliable measurements is to perform laboratory experiments in a wind-wave tank where more steady flow and scalar fields than oceans are attained and turbulence quantities can be more precisely measured. Although a number of laboratory experiments for investigating wind shear effects on the mass transfer have been conducted in a wind-wave tank, the effects of other factors such as fetch, swell and rain have not been fully clarified (Kurose et al., 2008; Takagaki & Komori, 2007; Sugioka & Komori, 2007). Furthermore, few heat transfer studies have been conducted to precisely measure the heat flux in a wind-wave tank.

The purpose of this study is to clarify the mechanism of heat and mass transfer across the wavy sheared air-water interface together with turbulence structure and to examine the conventional bulk models for estimating heat and mass transfer rates across the air-sea interface. By using the results obtained from laboratory measurements, we try to estimate the global heat and mass exchange rates between atmosphere and ocean.

EXPERIMENTS

Small and large wind-wave tanks were used here. The sketech of the tank is shown in Fig.1. The small (large) wind-wave tank had a glass test section of 7m (20m) long, 0.3m (0.6m) wide and 0.8m (1.3m) high. The water depth in the tank was 0.5m (0.7m) and the vertical height of the air flow above the air-water interface was 0.3m (0.6m). Nonlinear three-dimensional waves were driven in the wind-wave tanks by winds with the free-stream velocity of U_∞= 2 ~ 15m/s. Filtered tap water was mainly used and 3.5wt% salt water was also used to investigate the effect of salinity on heat and mass transfer.

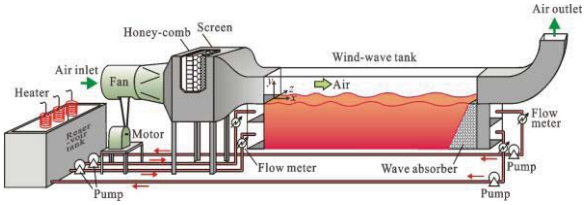

Figure 1: Exprimental apparatus.

Heat transfer experiments by evaporation were conducted only in a small wind-wave tank with warm water with a constant temperature of 40℃, since side and bottom walls were easily insulated by foam plates and temperature was easily controlled for the small tank compared to a large wind-wave tank. The measurements were carried out at x=4 m (fetch) from the entrance (x=0) into the test section. Instantaneous velocity and temperature were simultaneously measured at the same point using a laser Doppler velocimeter and cold film and wire I-probes operated by a constant-current temperature bridge in both air and water flows (Nagata and Komori, 2001) and turbulent heat flux was directly estimated from the simultaneous velocity and temperature measurements in the vicinity of the interface. Air velocity was also measured by a Particle Image Velocimetry (PIV) to obtain the vertical mean velocity profile. The surface temperature of the interface was measured by a high-speed scanning infrared thermometer and the humidty in the air flow was measured by an infrared hygrometer. In order to precisely estimate the frequency of the appearance of surface-renewal eddies in the water flow, f_S, a VITA technique was applied to the instantaneous vertical turbulent heat flux signal (Komori et al., 1993a). Instantaneous wave height was measured using a wave crest meter.

Mass transfer experiments were conducted through CO_2 desorption from the water side to the air side in both small and large wind-wave tanks. The large wind-wave tank enabled us to investigate the effect of the fetech on mass transfer. Pure CO_2 was excessively dissolved into filtered tap water at 20℃ in the tank, and the mean concentration of CO_2 in the air side was measured vertically at x =3, 4, 5, 7, 10 and 15m by using sampling tubes connected to CO_2 analyzers based on infrared spectroscopy. Mean concentration on the water side was measured by a sampling tube connected to a total organic carbon meter. Air velocity above the interface was measured by the PIV. By taking the mass balance from the vertical mean concentration and velocity profiles at the two stations of 3 and 5m in both small and large wind wave tanks, the mass flux F per unit area was estimated at x=4m and it was confirmed that F well agrees with the mass flux estimated by the flux profile method on the log-law profile of mean concentration. By means of this profile method, the mass transfer coefficient on the water side k_L was obtained for the fetches of x=7, 10 and 15m in a large tank by

$$k_L = F/\Delta C\,, \qquad (6)$$

where ΔC is the concentration difference between the interface and the bulk water. .

DIRECT NUMERICAL SIMULATION

Direct numerical simulation (DNS) was applied to investigate the relation between turbulence structure and scalar transfer in the wind speed less than 5m/s. Deforming wavy air-water interface was captured using an arbitrary Lagrangian Eulerian formulation (ALE) method with boundary-fitted coordinates (BFC). The numerical procedure used here was essentially the same as in Komori et al. (1993b). The non-dimensional equations governing the flow and passive mass in an incompressible Newtonian

fluid are the equation of continuity, Navier-stokes (N-S) equation, and conservation equation of passive mass:

$$\frac{\partial U_i}{\partial x_i} = 0 , \tag{7}$$

$$\frac{\partial U_i}{\partial t} + U_j \frac{\partial U_i}{\partial x_j} = -\frac{\partial p}{\partial x_i} + \frac{1}{Re} \frac{\partial^2 U_i}{\partial x_j \partial x_j} + \frac{1}{Fr} \delta_{i3} , \tag{8}$$

$$\frac{\partial C_i}{\partial t} + U_j \frac{\partial C_i}{\partial x_j} = \frac{1}{Re \cdot Sc} \frac{\partial^2 C}{\partial x_j \partial x_j} , \tag{9}$$

where U_i is the i th component of the velocity vector (i =1, 2 and 3 denote the streamwise, spanwise and vertical directions, respectively), p the pressure, δ_{ij} the kroneker's delta, C the passive mass. The Einstein summation convection is used. The non-dimensional parameters, Re, Sc and Fr based on the reference length L_0 and velocity U_0 are defined as

$$Re = \frac{U_0 L_0}{\nu} , \quad Sc = \frac{\nu}{D} , \quad Fr = \frac{U_0^2}{g L_0} , \tag{10}$$

where ν is the kinematic viscosity, D the molecular diffusivity of the mass, and g the acceleration of gravity.

On the free surface, two boundary conditions should be satisfied for the flow field as shown in Fig.2. One is the kinematic boundary condition that describes the Lagrangian behavior of the fluid particle on the free surface:

$$\frac{\partial f}{\partial t} + U_1 \frac{\partial f}{\partial x_1} + U_2 \frac{\partial f}{\partial x_2} = U_3 , \tag{11}$$

where f is the function representing the form of the free surface. The other is the dynamic boundary condition which is determined from the balance of stresses acting on the interface in the normal and tangential directions:

$$\begin{aligned} & p + \sigma_n + p_s = \tilde{p} + \tilde{\sigma}_n , \\ & \sigma_n = \frac{1}{Re} e_{ij} n_j n_i , \\ & p_s = \gamma \kappa_m , \end{aligned} \tag{12}$$

$$\begin{aligned} & \sigma_t = \tilde{\sigma}_t , \\ & \sigma_t = \frac{1}{Re} e_{ij} n_j t_i , \end{aligned} \tag{13}$$

where σ_n , σ_t , p_s , e_{ij} , γ , k_m n_i , t_i are the normal component of the viscous force vector, the tangential component of the viscous force vector, the pressure variation due to the surface tension, the deformation rate tensor, the surface tension, the mean curvature of the free surface, the unit vector in the normal direction and the unit vector in the tangential direction, respectively. The parameters with and without the tilde denote the values on the air and water sides, respectively. On the other hand, the passive mass conservation equation (9) was solved only on the water side. The boundary condition of the passive mass at the air-water interface on the water side was given by C = 1.0.

The governing equations (7)-(9) and (11) were discretized to construct the finite-difference formulation, and the marker and cell (MAC) method was used to solve the N-S equation. The discretization of the nonlinear terms in the N-S equation (8), the passive mass conservation equation (9) and the kinematic boundary condition (11) was derived from a fifth-order upwind scheme. The other spatial derivatives were approximated by a second-order central difference scheme. The time integration was carried out by an Euler implicit method.

The geometry and grid system of the computational domain are shown in Fig.3. The computational domain was 8 $\delta \times$ 4 $\delta \times$ 3 δ in the streamwise (x), spanwise (y) and vertical (z) directions. The origin ($x = y = z = 0$) was located at the height of 2 δ from the bottom, and the initial flat air-water interface which divides between the upper air and lower water sides was placed on the z = 0 plane. The grid points used in the streamwise (x), spanwise (y) and vertical (z) directions were 200 × 100 × 60 on the air side and 200 × 100 × 120 on the water side, respectively. The grid spacing was equidistant in the streamwise (x) and spanwise (y) directions, and to get high resolution the nonuniform meshes clustered in the air-water-interface region were used in the vertical (z) direction. Periodic boundary condition was applied in the streamwise (x) and spanwise (z) directions, and slip boundary condition was applied in the vertical (y) direction. As initial conditions of the flow field, a fully developed wall turbulent flow and a quiescent flow were given on the air and water sides of the flat interface, respectively. After the flow on the liquid side was fully developed, the boundary condition of the passive mass (C = 1.0) on the liquid side of the air-water interface was given.

Table 1 shows numerical conditions in this study. The parameters with the subscript "ini" in the table 1 indicate the initial values. The deforming air-water interface was simulated for an initial air uniform velocity $U_{\infty,ini}$ =5.2 m/s. The Reynolds number Re is based on the uniform air velocity U_∞ and the height of the computational domain on the air side (δ =1.25 × 10^{-2} m), and the Reynolds number Re_τ (= $\delta u^* / \nu$) is based on the friction velocity on the air side u^* and the height of the computational domain on the air side. The Schmidt number Sc was assumed to be unity in this study. This is because although the Schmidt number Sc in the liquid flows is generally much larger than unity ($Sc \simeq$ 600 for CO_2), DNS of such flows are impossible at present since the Batchelor scale which is a small-scale variation of passive scalar is much smaller than the Kolmogorov scale.

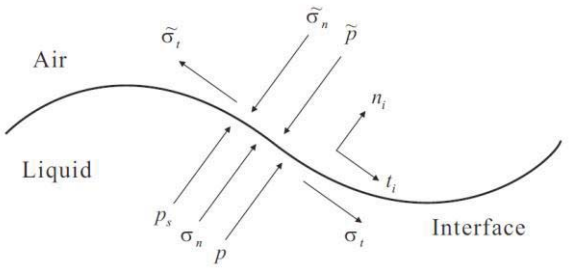

Figure 2: Boundary conditions at the air-water interface.

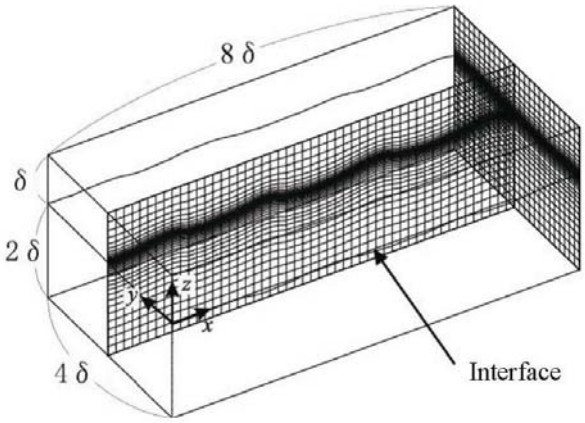

Figure 3: Computational domain and grids for DNS.

Table 1: Numerical conditions.

Interface	$U_{\infty,ini}$	u^*_{ini}	Re_{ini}	$Re_{\tau,ini}$
Deforming wave	5.2[m/s]	0.25	4340	205

RESULTS AND DISCUSSION

Heat Transfer

The total heat flux Q_T was estimated by $\rho_W C_{p,w} \overline{v\theta}|_{max}$, where $\overline{v\theta}|_{max}$ is the maximum value of the vertical turbulent heat flux $v\theta$ in the water flow just below the air-water interface. Heat transfer coefficient on the water side h_L was given by Eq.(2). Figure 4 shows the distribution of h_L against the free-stream wind speed U_∞. The coefficient h_L increases with U_∞, and its profile has a small plateau in the middle wind speed region of 7.5~10m/s. When the surface temperature distributions taken by a high-speed scanning infrared thermometer are compared between two cases of U_∞=3.1m/s and 13.2m/s as shown in Fig. 5, it is found that the surface flow pattern changes from streaky structure and patchy one. Corresponding to this transition, the standard deviation of surface temperature σ_T also has a plateau in the middle wind speed region as shown in Fig.6.

In the low wind speed region, the turbulence structure is close to the structure on the flat boundary layer. In fact, the DNS predictions of the instantaneous mass flux on the air-water interface at $U_{\infty,ini}$ = 5.2 m/s in Fig. 7 and the instantaneous iso-surfaces of the second invariant on the water side in Fig.8 show the streaky structure and the appearance of typical horseshoe vortices beneath the streakes. Although it is impossible to numerically simulate the turbulence structure at higher wind speed than 10m/s where breaking waves are actively generated, the longitudinal turbulence structure may be disturbed by the ripple-like breaking waves in such high wind speed region. Thus, the patchy structure may appear in the high wind speed region by mixing of the longitudinal horseshoe vortices with spanwise ripple-like vortices. In the middle wind speed region of U_∞=7.5~10m/s corresponding to the trandition region, waves are developed with increasing U_∞ and the friction velocity increases with U_∞. However, in the transition region the increase of the shear stress at the interface (friction drag) may be suppressed by the flow separation behind wave crests in contrast to the increase of the form drag (pressure drag). In fact, the frequency of the appearance of surface-renewal eddies in the water flow, f_S, which was estimated by applying a VITA technique to instantaneous vertical heat flux $v\theta$, has a similar trend to h_L in Fig.9. This explains why h_L has a small plateau in the middle wind speed region.

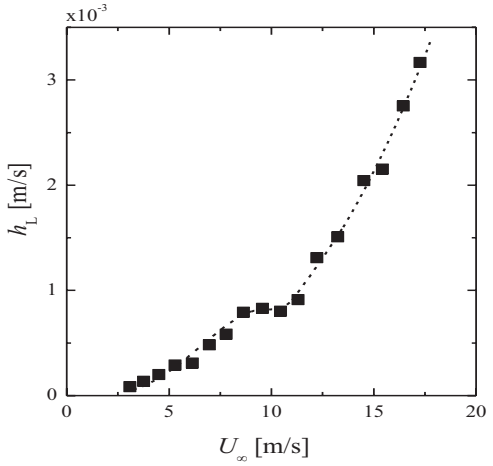

Figure 4: Heat transfer coefficient on the water side h_L against U_∞.

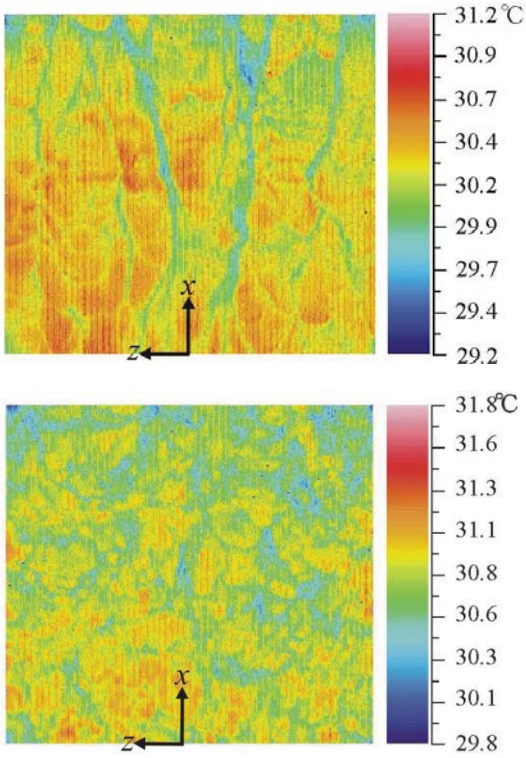

Figure 5: Instantaneous surface temperature at U_∞ =3.1m/s (upper) and 13.2m/s (lower).

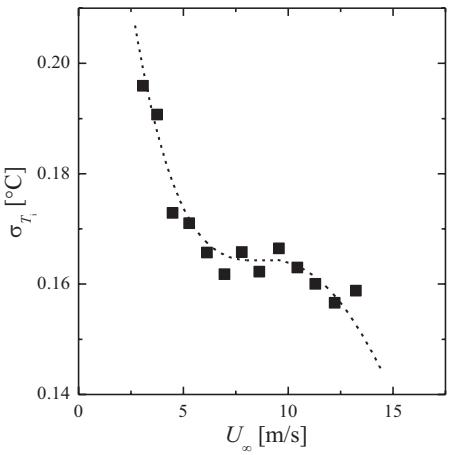

Figure 6: Standard deviation of surface temperature against U_∞.

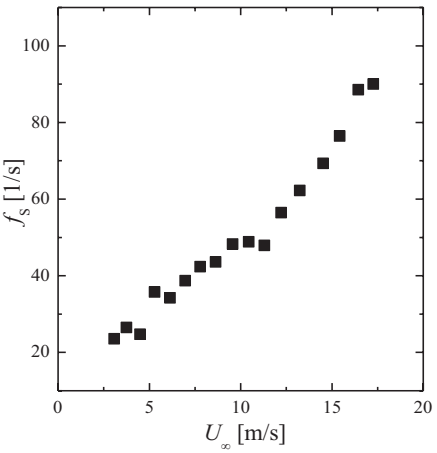

Figure 9: Frequency of the appearance of surface-renewal eddies in the water flow f_S against U_∞.

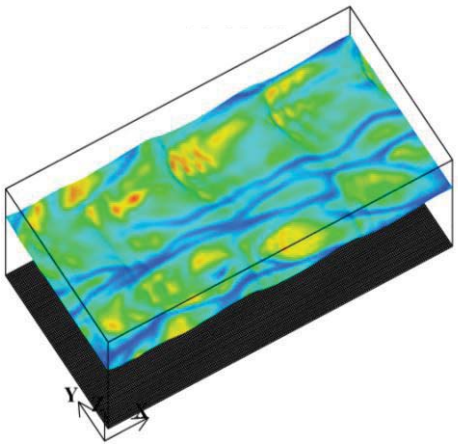

Figure 7: Instantaneous mass flux at the air-water interface by DNS.

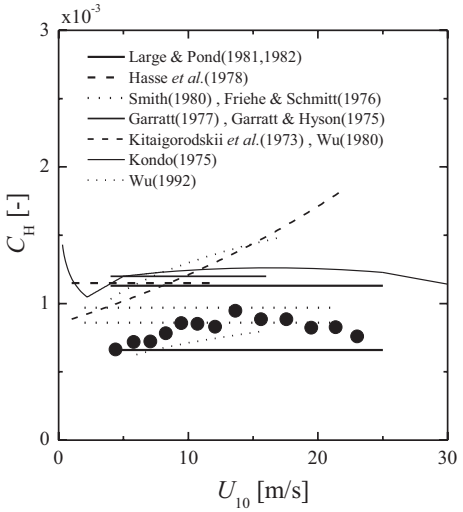

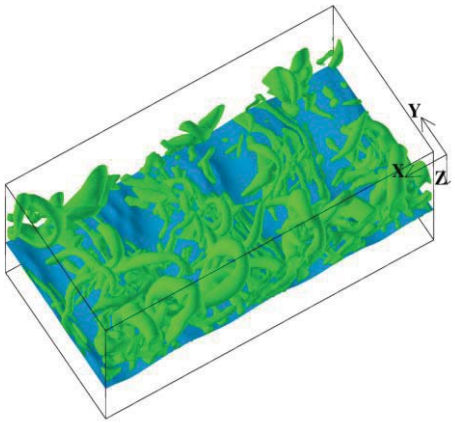

Figure 8: Instantaneous iso-surfaces of the second invariant on the water side by DNS.

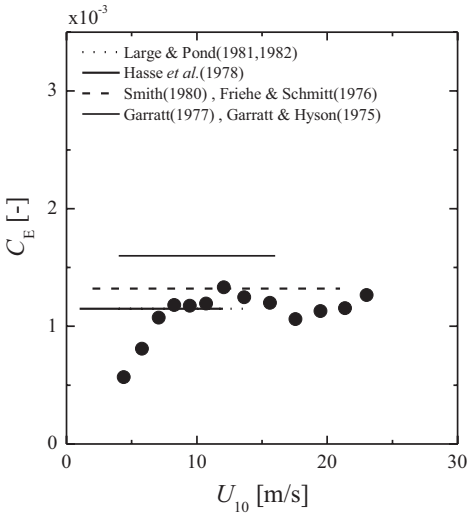

Figure 10: Heat flux transfer coefficients C_H and C_E against U_{10}.

In order to estimate C_H and C_E in Eqs.(4) and (5), the sensible heat flux Q_H was estimated by $\rho_a C_{p,a} \overline{v\theta}|_{max}$, where $\overline{v\theta}|_{max}$ is the maximum value of the vertical turbulent heat flux $v\theta$ in the air flow just above the air-water interface. Radiative heat flux Q_R in Eq.(3) was estimated by the Stefan-Boltzmann law. From these Q_H and Q_R together with Q_T measured in the water flow, the latent heat flux Q_E was calculated using Eq.(3).

Figure 10 shows the distributions of sensible and latent heat flux transfer coefficients C_H and C_E obtained by substituting the above Q_H and Q_E into Eqs.(4) and (5) against U_{10}, together with the best-fittong curves of previous field measuements. The sensible heat flux transfer coefficient C_H is almost constant irrespective of the wind speed, but it is smaller than the field measurements. Wheras C_E shows the complicated depedence of wind speed and it differes from the field measurements. This suggests that the conventional assumption for the same constant value around unity for C_H and C_E is not suitable for estimating the heat flux on the air side. Instead of such transfer coefficients, we propose the following sensible and latent heat transfer coefficients h_A and k_A:

$$Q_H = \rho_a C_{p,a} h_A \Delta T , \tag{14}$$

$$Q_E = \rho_a L_V k_A \Delta q , \tag{15}$$

where ΔT and Δq are the temperture and humidty differences between the bulk air flow and the interface. Figure 11 shows the distributions of h_A and k_A against the free stream wind speed U_∞. The coefficient h_A is proportional to U_∞, and k_A shows very similar behavior to the heat transfer coefficient on the water side h_L in Fig.4. This suggests that sensible heat transfer is controlled by the air turbulence, and the latent heat transfer dominates the total heat transfer across the air-water interface.

Mass Transfer

Figure 12 shows the distributions of the mass transfer coefficient on the water side k_L against the free-stream wind speed U_∞, at fetches of x=4, 7, 10 and 15m in a large tank and x=4m in a small tank. The values of k_L in the present small and large wind-wave tanks are well correlated with U_∞ irrespective of fetch. The distributions also have a small plateau in the middle wind speed region as well as h_L, and they differ from the conventional monotonous increasing k_L. This means that the mass transfer is also controlled by the same mechanism as the heat transfer. It was also found that k_L is a little better correlated by U_∞ than by air friction velocity u^*_a or wind speed at the elevation of 10m above the air-water interface, U_{10}.

In order to investigate the effect of salinity on the mass transfer, the same CO_2 transfer experiments were conducted in the small wind-wave tank with 3.5wt% salt water. Figure 13 shows the ratio of the mass transfer coefficient for the salt water to that for the fresh water, k_{LS}/k_{LF}. The effect of salinity appears in low and middle wind speed region less than 8m/s. The damping effect may be caused by the apparent reduction of molecular diffusivity due to surface contamination (Komori & Shimada, 1995). Such damping effect was not found in heat transfer.

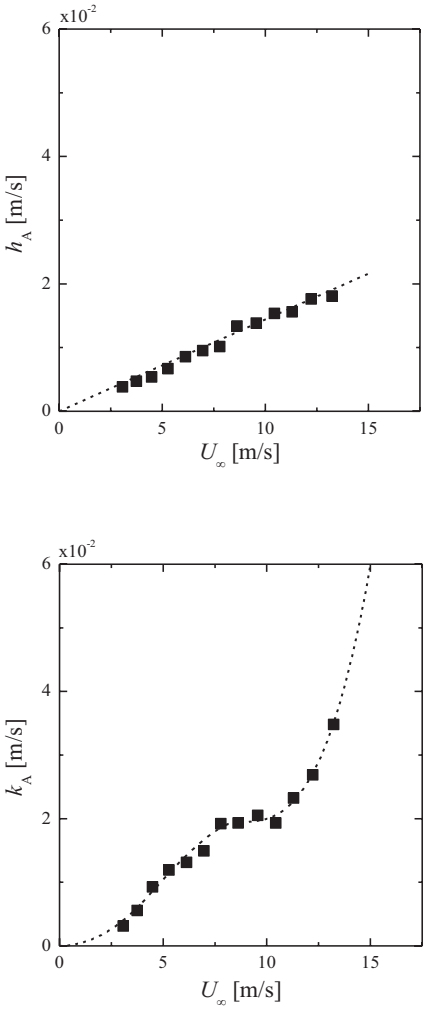

Figure 11: Distributions of h_A and k_A against U_∞.

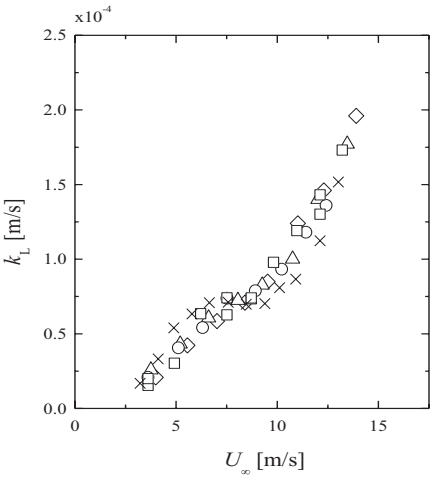

Figure 12: Mass transfer coefficient on the water side k_L against U_∞: □, ○, Δ, ◊ at x=4, 7, 10 and 15m in a large wind-wave tank, respectively; × at x=4.0m in a small wind-wave tank.

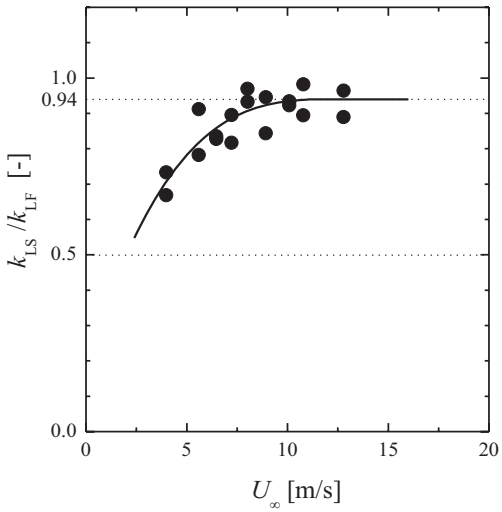

Figure 13: The ratio of the mass transfer coefficient for the 3.5wt% salt water to that for the fresh water k_{LS}/k_{LF} against U_∞.

Global Air-Sea Heat and Mass Transfer

It is of interest to estimate the global heat and mass exchange rates between atmosphere and ocean by using the above laboratory measurements. Figure 14 shows the comparison of the present k_L with field measurements by the eddy-correlation method (McGillis et al., 1997, 2001, 2004; Fairall et al., 2000; Jacobs et al., 2002). Here the present k_L is given by multiplying k_L in Fig.12 by the damping factor in Fig.13 and all the data are plotted against U_{10}. It is found that the present measurements remarkably deviate from the field data in the middle and high wind speed region. This suggests that U_{10} is not a suitable parameter for correlating k_L. On the other hand, the field measurements plotted against the free stream wind speed U_∞ come to the present measurements as shown in Fig.15. Here the free stream wind speed at the outer edge of the atmospheric boundary layer above the air-sea interface was approximately given by the wind speed at the elevation of 65m (Anderson et al., 2005; Toba et al., 1990).

The field measurements are so scattered that it is difficult to show explicitly the availability of U_∞. However, the agreement with the field data suggests that the outer variable U_∞ may be a more suitable parameter for correlating k_L than inner variables such as u^*_a or U_{10}. When we consider the wavy interface as a kind of roughness boundary, the approximate proportionality between the frequency of the appearance of surface-renewal eddies f_S and U_∞ (see Fig.9) also suggests that the surface-renewal frequency closely affecting k_L is determined only by U_∞ irrespective of the Reynolds number and the bounday layer thickness. In fact, the ratio of the free-stream wind speed to bursting frequency measured by Antonia & Krogstad (1993) and Mochizuki & Ohsaka (1992) in a rough bounday layer in a wind tunnel shows an almost constant value irrespective of Reynolds number and boundary layer thickness. When we consider the close relation between orgnized motions above and below the interface (Komori et al., 1993a), we can accept the correlation between k_L and U_∞ in Fig.15.

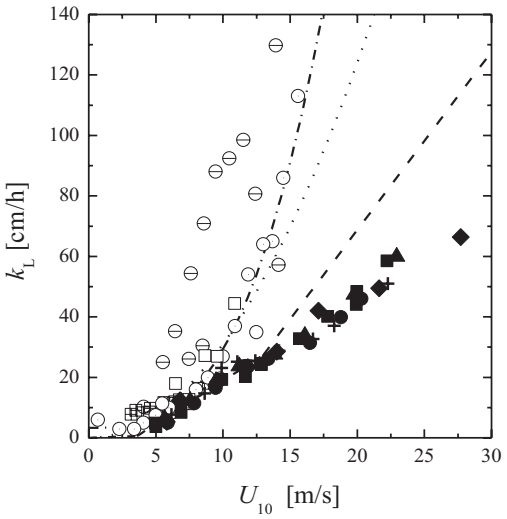

Figure 14: Comparison of k_L with field measurements against U_{10}. Closed and open symbols are the present laboratory measurements and previous field measurements, respectively. Lines show the conventional k_L models by; - - - - Liss & Merlivat (1986); ------ Wanninkhof et al. (1992); - - - - -- McGillis et al. (2001).

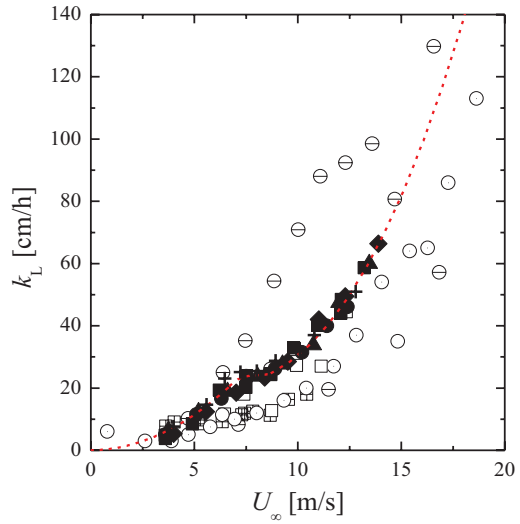

Figure 15: Comparison of k_L with field measurements against U_∞. Symbols as in Fig.14.

Under the assumption that k_L is given by a dashed line in Fig.15, we can estimate the global carbon exchange rate using the data base of ΔpCO_2 (Takahashi et al., 2002) and wind speed from NCEP/NCAR (National Center for Environmental Prediction/National Center for Atmospheric Research) Reanalysis (Kalnay et al., 1996). Figure 16 shows the distribution of mean annual air-sea CO_2 flux for year 2001. It is found that uptake and discharge of CO_2 into and from oceans are seen in high and low latitude regions, respectively. Table 2 also shows the global CO_2 exchange rate for year 2001 with the predictions by previous models in Fig.14 (Liss & Merlivat, 1986; Wanninkhof et al., 1992; McGillis et al., 2001). The present model of k_L shows that the net uptake of carbon into the oceans is about 2.2 PgC/year and this value well agrees with the value estimated by the IPCC report (2007), compared to other predictions .

For heat transfer, it is not easy to estimate the global exchange rate as well as mass transfer. If the temperature difference between the ocean surface and bulk water is precisely given by the database, the global heat flux can be estimated using h_L in Fig.4 as well as the mass flux. However, the temperature difference on the water side is too small to precisely estimate the total heat flux Q_T in Eq.(2) by h_L. Therefore, the heat transfer rate has been estimated only on the air side by using Eqs.(3)-(5). When the conventional heat flux transfer coefficients (C_H=C_E=0.00125) against U_{10} are used with the NCEP/NCAR Reanalysis air temperature and humidty data sets, the global mean air-sea sensible and latent heat fluxes Q_H and Q_E are estimated to be 11.5 W/m^2 and 95.0W/m^2, respectively. If we use sensible and latent heat transfer coefficients h_A and k_A against U_∞ in Fig.11 together with the temperture and humidty differences between ocean surface and measuement points given in the NCEP/NCAR Reanalysis air temperature and humidty data sets, we obtain the heat fluxes of Q_H=12.1W/m^2 and Q_E= 182W/m^2. The latent heat flux is rather larger than the conventional estimation. However it should be noted that the present simulation of global heat transfer is based on the uncertain estimation of temperture and humidty differences between atmosphere and ocean.

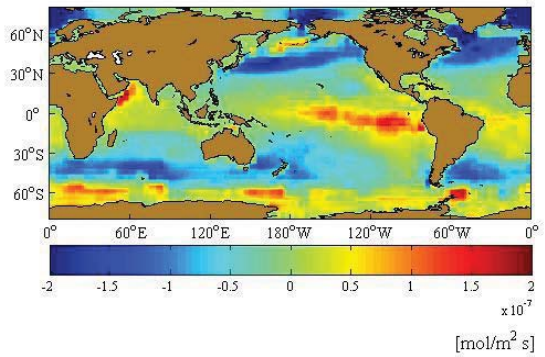

Figure 16: Distribution of mean annual air-sea CO_2 flux for year 2001.

Table 2: Global CO_2 exchange rate for year 2001 estimated by some correlations between k_L and U_∞ or U_{10}. The unit of the exchange rate is PgC/year.

Authors	Net	Sea to Air	Air to Sea
This study for k_L vs. U_∞	-2.19	2.5	-4.69
McGillis et al. (2001) for k_L vs. U_{10}	-1.59	1.52	-3.11
Wanninkhof et al. (1992) for k_L vs. U_{10}	-1.39	1.55	-2.94
Liss & Merlivat (1986) for k_L vs. U_{10}	-0.80	0.93	-1.73

CONCLUSIONS

Heat and mass transfer mechanism across the sheared air-water interface was both experimentally and numerically investigated. Turbulence structure near the interface was clarified by instantaneous velocity and temperature measurements together with direct numerical simulation of wind-driven turbulence. The main results from this study can be summarized as follows.

Both heat and mass transfer coefficients on the water side increase with the free-stream wind speed and they have a small plateau in the middle wind speed region where the streaky flow structure changes to patchy one. The distributions of the mass transfer coefficient against the free-stream wind speed also show no dependency of fetch and they agree with the field measurements plotted against the free-stream wind speed in the atmospheric surface layer. The assumption that sensible and latent heat flux transfer coefficients have the same constant value is not appropriate to the conventional bulk models and new transfer coefficients are proposed in this study.

ACKNOWLEDGEMENTS

The authors thank N. Takagaki, K. Handa, T. Kobayashi, T. Ukai for their great help in conducting experiments and numerical calculations, and Emeritus Prof. Y. Toba of Tohoku University and Prof. W. McGillis of Columbia University for their kind suggestions on turbulence structure and mass flux measurements. This work was supported by the Ministry of Education, Science, Sports and Culture, Grant-in Aid (No. 19206023).

REFERENCES

Anderson, P. S., Ladkin, R. S., and Renfrew, I. A., 2005, "An autonomous Doppler sodar wind profiling system", *J. Atmos. Oceanic Technol.,* Vol. 22, pp. 1309–1325.

Antonia, R. A., and Krogstad, P. A., 1993, "Scaling of the bursting period in turbulent rough wall boundary layers", *Exp. Fluids*, Vol. 15, pp. 82-84.

DeCosmo, J., Katsaros, K. B., Smith, S. D., Anderson, R. J., Oost, W. A., Bumke, K., and Chadwick, H., 1996, "Air-sea exchange of water vapor and sensible heat: The Humudity Exchange Over the Sea (HEXOS) results", *J. Geophys. Res.*, Vol. 101, pp. 12001–12016.

Fairall, C. W, Hare, J. E., Edson, J. B., and McGillis,

W., 2000, "Parameterization and micrometeorological measurement of air-sea gas transfer", *Boundary-Layer Meteorology*, Vol. 96, pp. 63–105.

Garratt, J. R., 1977, "Review of drag coefficients over oceans and continents", *Mon. Wea. Rev.*, Vol. 105, pp. 915-929.

Hasse, L., Grunewald, M., Wucknitz, J., Dunckel, M., and Schriever, D., 1978, "Profile derived turbulent fluxes in the surface layer under disturbed and un disturbed conditions during GATE", *Meteor Forschungsergeb*, Vol. 13, pp. 24-40.

IPCC, 2007: *Climate Change 2007: The Physical Science Basis. Contribution of Working Group I to the Fourth Assessment Report of the Intergovernmental Panel on Climate Change.*

Kalnay, E., Kanamitsu, M., Kistler, R., Collins, W., Deaven, D., Gandin, L., Iredell, M., Saha, S., White, G., Woollen, J., Zhu, Y., Leetmaa, A., Reynolds, R., Chelliah, M., Ebisuzaki, W., Higgins, W., Janowiak, J., Mo, K. C., Ropelewski, C., Wang, J., Jenne, R., and Joseph, D., 1996, "The NCEP/NCAR 40-year reanalysis project", *Bull. Amer. Meteor. Soc.*, Vol. 77, pp. 437-470.

Kitaigorodskii, S. A., Kuznetsov, A., and Panin, G. N., 1973, "Coefficients of drag, sensible heat, and evaporation in the atmosphere over the surface of the sea", *Izv. Acad. Sci. USSR, Atmos. Ocean. Phys*., Vol. 9, pp. 644-647.

Komori, S., Nagaosa, R., and Murakami, Y., 1993a, "Turbulence structure and mass transfer across a sheared air-water interface in wind-driven turbulence", *J. Fluid Mech.*, Vol. 249, pp. 161–183.

Komori, S., Nagaosa, R., Murakami, Y., Chiba, S., Ishii, K., and Kuwahara, K., 1993b, "Direct numerical simulation of three-dimensional open-channel flow with zero-shear gas-liquid interface", *Phys.Fluids,* Vol. A5, pp. 115-125.

Komori, S., and Shimada, T., 1995, "Gas transfer across a wind-driven air-water interface and the effects of sea water on CO_2 transfer", *Air-Water Gas Transfer* Eds. B.Jahne & E.C. Monahan, AEON Verlag, pp. 553-569.

Large, W. G., and Pond, S., 1982, "Sensible and latent heat flux measurements over the ocean", *J. Phys. Oceanogr*., Vol. 12, pp. 464-482.

Liss, P. S., and Merlivat, L., 1986, "Air-sea gas exchange rates: introduction and synthesis", *The Role of Air-Sea Exchange in Geochemical Cycling,* pp. 113–127.

McGillis, W. R., and Edson, J. B., 1997, "An investigation of gas transfer voefficients using direct estimates of the CO_2 flux", *WHOI, Woods Hole Oceanographic Institute*, 18pp.

McGillis, W. R., Edson, J. B., Hare, J. E., and Fairall, C. W., 2001, "Direct covariance air-water CO_2 fluxes", *J. Geophys. Res.*, Vol. 106, pp. 16729–16745.

McGillis, W. R., Edson, J. B., Zappa, C. J., Ware, J. D., McKenna, S. P, Terray, E. A., Hare, J. E., Fairall, C. W., Dorennan, W., Donelan, M. De-Grandpre, M. D., Wanninkhof, R., and Feely, R. A., 2004, "Air-sea CO_2 exchange in the equatorial Pacific", *J. Geophys. Res.*, Vol. 109, C08S02, doi:10.1029/2003JC002256.

Mochizuki, S. and Osaka, H., 1992, "Coherent structure of a d-type rough wall boundary layer in a transitionally rough and a fully rough regime", *Trans. of JSME (B)*, Vol. 58, pp. 1392-1399.

Nagata, K., and Komori, S., 2001, "Difference in Turbulent Diffusion between Active and Passive Scalars in Stable Thermal Stratification", *J. Fluid Mech.*, Vol.430, pp.361-380.

Pedreros, R., Dardier, G., Dupuis, H., Graber, H. C., Drennan, W. M., Weill, A., Guerin, C., and Nacass, P., 2003, "Momentum and heat °uxes via the eddy correlation method on the R/V L'Atalante and an ASIS buoy", *J. Geophys. Res.*, Vol. 109, C11, 3339.

Sugioka, K.I. and Komori, S., 2007, "Drag and lift forces acting on a spherical water droplet in homogeneous linear shear air flow", *J. Fluid Mech.*,Vol.570 , pp.155 – 175.

Smith, S. D., 1980, "Wind Stress and Heat Flux Over the Ocean in Gale Force Winds", *J. Phys. Oceanogr.*, Vol. 10, pp. 709-726.

Takahashi, T., Surherland, S. C., Sweeney, C., Poisson, A., Metzl, N., Tilbrook, B., Bates, N., Wanninkhof, R., Feely, R. A., Sabine, C., Olafsson, F., and Nojiri, Y., 2002, "Global sea-air CO_2 flux based on climatological surface ocean pCO_2, and seasonalbiological and temperature effects", *Deep-Sea Research II*, Vol. 49, pp. 1601–1622.

Toba, Y., Iida, N., Kawamura, H., Ebuchi, N., and Jones, I.S.F., 1990, "Wave dependence of sea-surface wind stress", *J. Phys. Oceanogr.*, Vol. 20, pp. 705–721.

Wanninkhof, R. H., 1992, "Relationship between wind speed and gas exchange over the ocean", *J. Geophys. Res.*, Vol. 97, pp. 7373–7382.